Stability of viscous fingering

David Bensimon
Department of Physics and The James Franck Institute, University of Chicago, 5640 South Ellis Avenue, Chicago, Illinois 60637
(Received 10 May 1985; revised manuscript received 21 August 1985)

Flows in a two-dimensional Hele-Shaw cell are studied analytically and numerically by conformal-mapping methods. In the presence of surface tension the fingers are linearly stable. However, the structure of the linear stability problem is exponentially sensitive to noise, which implies the existence of a finite-amplitude nonlinear instability appearing at low surface tensions. Numerical simulations demonstrate the existence of this instability. The most unstable modes are predicted and compared with real and numerical experiments.

I. INTRODUCTION

The flow of two immiscible fluids in a Hele-Shaw cell[1] is an interesting problem which exemplifies many of the features observed in pattern formation processes: emergence of an ordered structure from a transient chaotic regime, and (upon variation of some control parameters) bifurcation of that selected state into an oscillatory and eventually chaotic one. Indeed when a viscous fluid confined between closely spaced parallel sheets of glass (a Hele-Shaw cell) is driven by a less viscous one, the interface between the fluids is unstable. It develops a transient chaotic pattern of fingerlike invaginations from which a single propagating finger emerges, which width is experimentally related to the driving velocity. Upon increasing that velocity the propagating finger is first observed to bifurcate to an oscillatory state and eventually a chaotic state may be achieved.

The theoretical model describing the flow in a Hele-Shaw cell[2] belongs to the class of the two-dimensional Stefan problems: in the quasistationary limit it involves solving the Laplace equation for some field ϕ with boundary values specified on a moving interface Γ, the velocity of which is in turn determined by the gradient of ϕ. It has some very puzzling riddles. (1) In the absence of surface tension, Saffman and Taylor[2] showed that there exists a continuous family of steady-state solutions, i.e., penetrating fingers parametrized by their relative width λ. In the presence of surface tension, a formal singular perturbation analysis by McLean and Saffman[3] seems to show that the continuous family of solutions persists. However, numerical solutions of the steady-state equations[3,4] show no hint of the continuous family. Rather,[4] the analysis indicates a countably infinite discrete family of steady-state propagating fingers. (2) Results of linear stability analysis of the $\lambda=\frac{1}{2}$ finger are contradictory[3,5] and neither show the experimentally observed transition to an unstable propagating finger at low surface tension (high velocities).[2,6]

It is the purpose of this paper to describe a method, which is well suited for efficient numerical studies addressing the questions raised above, and which can be applied successfully to the analytical study of this problem and related Stefan problems[7] (solidification, dendritic growth, electrodeposition, etc.). In particular it allows one to address the problem of the stability of the $\lambda=\frac{1}{2}$ finger from a new perspective, and thus to solve it. In the following we will first describe the interface dynamics approach as developed by Shraiman and Bensimon.[7] We will look for steady-state solutions both with and without surface tension. We will then study the linear stability of one of these solutions: the $\lambda=\frac{1}{2}$ finger, which is the one experimentally observed at high velocities. In the absence of surface tension it is unstable, as first noticed by Saffman and Taylor.[2] In the presence of surface tension this finger is linearly stable, a conclusion reached independently by Kessler and Levine[5] using a different (numerical and thus less accurate) approach. However, the spectral structure of the linear operator, which eigenvalues determine the stability of the steady-state interface, is exponentially sensitive to noise. Namely the amplitude of the perturbation necessary to destabilize the finger decreases as an exponential power of the velocity. We relate that structural sensitivity to a finite amplitude nonlinear instability of the interface and are then able to predict the form of the most nonlinearly unstable modes. Results of numerical simulations based on this method demonstrate the existence of a noise-driven nonlinear instability, and support the results of our analysis.

II. INTERFACE DYNAMICS

The Saffman-Taylor equations[2] describe the fluid velocity $\mathbf{v}$ in terms of a velocity potential ϕ ($\mathbf{v}=\nabla\phi$) which obeys the Laplace equation

$$\nabla^2\phi=0\ , \tag{1a}$$

with the following boundary conditions at the interface:

$$\phi\,|_\Gamma=d_0\kappa\,|_\Gamma\ , \tag{1b}$$

$$(\nabla\phi)_n=\left[\frac{\partial\Gamma}{\partial t}\right]_n\ , \tag{1c}$$

where Γ is the interface between the two fluids which evolution we want to track, κ its curvature, n indicates a direction normal to the interface, and d_0 is the dimensionless surface-tension parameter. In terms of measurable quantities d_0 is given by

$$d_0=\frac{1}{12}\left[\frac{2\pi b}{W}\right]^2\frac{T}{\mu V}\ , \qquad (2)$$

where b is the cell thickness, W its width (in this paper for convenience $W=2\pi$), T the surface tension, μ the viscosity of the driven fluid, and V its velocity at infinity. [Since there is no agreement on the exact form of the surface-tension parameter we will, for the convenience of the reader, relate our parameter d_0 to the one used by others. Thus the parameter κ used by McLean and Saffman[3] is $\kappa=d_0\lambda/(1-\lambda)^2$. The parameter B introduced by Tryggvason and Aref[8] is $B=d_0/(2\pi)^2$. Finally, the critical unstable wavelength for a flat interface is $\lambda_c=W\sqrt{d_0}$.] In principle, Eq. (1) should be supplied with boundary conditions on the walls, i.e., the normal component of the velocity equals zero; however, we will assume here periodic boundary conditions which correspond to a cylindrical Hele-Shaw cell such as the one used by Aribert.[9]

Equations (1a)–(1c) determine the evolution of the interface: the Laplace equation with the Dirichlet boundary condition on Γ, Eq. (1b), completely determines the flow field, then the value of the normal velocity (the normal component of ϕ) at the boundary determines the velocity of the interface, Eq. (1c). We have to solve a Stefan, or moving-boundary-value problem. The two dimensionality of the problem greatly simplifies the task by allowing the use of the conformal-mapping technique.

The idea which is standard in all textbooks on complex variables[10] is based on the Riemann mapping theorem. This theorem ensures the existence of a conformal map from the complicated but simply connected domain enclosed by the interface Γ into a standard domain, the interior of the unit disk. Within the disk the Dirichlet problem for the potential ϕ, Eqs. (1a) and (1b) can be readily solved. That solution then enables us to rewrite Eq. (1c) as an evolution equation for the mapping. We introduce the complex potential

$$\Phi(w)=\phi(x,y)+i\psi(x,y)\ ,$$

which is an analytic function of $w=x+iy$. We then conformally map the domain of interest, i.e., the space occupied by the driven fluid into the unit disk [$|z|\le 1$, $z=f_t^{-1}(w)$]; see Fig. 1. Since the interface Γ between the two fluids is the image of the unit circle ($z=e^{is}$) under the map $f_t(z)$,

$$\Gamma(t,s)=f_t(e^{is})\ , \qquad (3)$$

specifying the mapping $f_t(z)$ at a given time t is identical to specifying the interface $\Gamma(t,s)$ and its parametrization s.

The solution of Eqs. (1a) and (1b) in the z plane (inside the unit disk) is standard.[10] One has to determine the function analytic inside the unit disk $\Phi(z)$ which real part on its boundary ($z=e^{is}$) is specified: $\phi(s)=d_0\kappa(s)$, where $\kappa(s)$, the curvature of $\Gamma(t,s)$, is

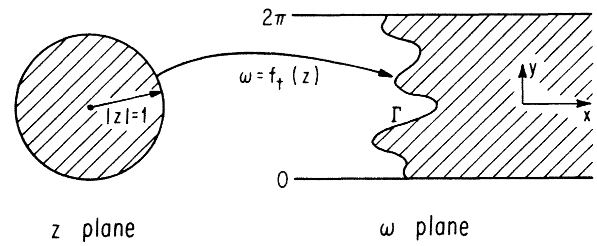

FIG. 1. Conformal map from the unit disk to the space occupied by the driven fluid.

$$\kappa(s)=-\frac{\mathrm{Im}(\partial_s^2 f/\partial_s f)}{|\partial_s f|}\ . \qquad (4)$$

The solution is known to be given by the Poisson integral formula.[10] That formula states that the function analytic for $|z|<1$, $\tilde{g}(z)$, for which the real part on the unit disk $g(s)$ can be written as

$$g(s)=a_0+\sum_{n=1}^{\infty}(a_n e^{ins}+a_n^* e^{-ins})\ , \qquad (5)$$

must be

$$\tilde{g}(z)\equiv A\{g(s)\}=a_0+2\sum_{n=1}^{\infty}a_n z^n\ . \qquad (6)$$

Therefore, the potential $\Phi(z)$ inside the unit disk is

$$\Phi(z)=-\ln z+d_0\tilde{\kappa}(z)\ . \qquad (7)$$

The first term on the right-hand side of that equation ($-\ln z$) is the solution for the potential in the absence of surface tension ($d_0=0$). Notice that since we are mapping the unit disk into the strip $0\le y<2\pi$, in the limit $x\to\infty$, $w\to-\ln z$. Thus Eq. (7) implies that the velocity of the fluid far away in front of the interface ($x\to\infty$) is normalized to 1. Now, the normal velocity of the interface, given by Eq. (1c) is

$$\left[\frac{\partial\Gamma}{\partial t}\right]_n=\left[\frac{\partial f}{\partial t}\right]_n=\hat{n}\partial_n\Phi\ , \qquad (8)$$

where

$$\hat{n}=i\frac{\partial_s f}{|\partial_s f|}=-\frac{z\partial_z f}{|z\partial_z f|}\ ,$$

$$\partial_n\Phi=\mathrm{Re}(n\partial_w\Phi)$$

$$=-\frac{\mathrm{Re}(z\partial_z\Phi)}{|z\partial_z f|}=\frac{1-d_0\,\mathrm{Re}[z\partial_z\tilde{\kappa}(z)]}{|z\partial_z f|}\ .$$

This equation specifies only the normal velocity of the interface. There is, of course, no physical significance to a tangential velocity which would simply correspond to a reparametrization of the interface. However, the analyticity of the mapping function $f_t(z)$ fixes a particular "analytic" parametrization "gauge" which has to be maintained for all time.[7] To achieve that, it is sufficient to make the time derivative of the map $\partial_t f$ analytic inside the unit disk. For that purpose we add to the right-hand side of Eq. (8) an appropriate tangential velocity component $i\hat{n}C'$,

$$\frac{\partial f}{\partial t}=\hat{n}\partial_n\Phi+i\hat{n}C'=z\partial_z f\left[\frac{\mathrm{Re}(z\partial_z\Phi)}{|z\partial_z f|^2}+iC\right]_{z=e^{is}}, \tag{9}$$

where C and C' are real functions of z. For the evolution of $f_t(z)$ to be analytic the terms in the large parentheses must describe an analytic function (thus C has to be the harmonic conjugate of the first term in the large parentheses). In other words, they have to represent the function analytic in $|z|\leq 1$, which real part on $|z|=1$ is specified $[=\mathrm{Re}(z\partial_z\Phi)/|z\partial_z f|^2]$. We have seen previously that this is achieved by the Poisson integral formula as expressed in Eqs. (5) and (6). One thus obtains the desired evolution equation for the mapping:

$$\frac{\partial f}{\partial t}=-z\partial_z f A\left[\frac{1-d_0\,\mathrm{Re}[z\partial_z\tilde{\kappa}(z)]}{|z\partial_z f|^2}\right], \tag{10}$$

where the integral operator A has been defined in Eq. (6). Equation (10) serves as the basis of the numerical scheme for the evolution of the interface, as well as for the linear stability analysis, which shall be presented in the following. However, before studying time-dependent states, we will look for steady-state solutions of Eq. (1).

III. STEADY-STATE SOLUTIONS

Steady states are characterized by an interface propagating unaltered along the cell at a velocity U, i.e., $d\Gamma/dt=U\hat{x}$. To find such states it is easier to recast Eq. (1c) in the following form:

$$\mathrm{Re}(n\partial_w\Phi)\equiv\partial_n\Phi\,|_\Gamma=Un_x\,|_\Gamma\equiv U\,\mathrm{Re}(n)\ . \tag{11}$$

It is then straightforward to show that

$$\mathrm{Re}(z\partial_z\Phi)_{z=e^{is}}=U\,\mathrm{Re}(z\partial_z f)_{z=e^{is}}\ . \tag{12}$$

In the absence of surface tension ($\Phi=-\ln z$), one obtains the Saffman-Taylor one-parameter family of solutions:[2]

$$f_0(z)=2(1-\lambda)\ln(z-1)-\ln z\ , \tag{13}$$

where $\lambda(=1/U)$ is the relative width of the propagating finger (the width of the finger divided by the width of the channel). In the presence of surface tension [Φ given by Eq. (7)], the formal solution is

$$f(z)=f_0(z)+d_0\lambda\tilde{\kappa}(z)\ . \tag{14}$$

Since $\tilde{\kappa}(z)$ is a functional of $f(z)$, Eq. (14) is a functional fixed-point equation for the mapping $f(z)$, which, in principle, can be solved recursively. This functional equation may be a clue to the understanding of the mentioned discrepancy between the singular perturbation analysis of McLean and Saffman[3] and their numerical results.[3,4] Namely the solution of Eq. (14), expressed as an expansion in d_0, may converge to different fixed points, $f^*(z)$ [depending on the initial "guess" $f(z)$] corresponding to the different members of the discrete family of solutions obtained numerically.[4]

IV. LINEAR STABILITY ANALYSIS

We shall now present the results of the linear stability analysis for the $\lambda=\frac{1}{2}$ finger which is the one observed in the limit $d_0\to 0$ (low surface tensions or high velocities). As usual we will assume that the mapping $f_t(z)$ can be written as

$$f_t(z)=f_0(z)+\eta(z)+\epsilon_t(z)\ , \tag{15}$$

where $f_0(z)$ is the $d_0=0$ Saffman-Taylor steady-state solution, $\eta(z)$ is a small time-independent correction to the shape of the interface, and $\epsilon_t(z)$ is a small time-dependent perturbation. Since $f_t(z)$ is analytic inside the unit disk we may assume

$$\eta(z)=\sum_{m=0}^{\infty}\eta_m z^m\ ,\qquad \epsilon_t(z)=\sum_{n=0}^{\infty}\epsilon_n(t)z^n\ . \tag{16}$$

In principle, the shape-correction term $\eta(z)$ is a small surface tension effect of $O(d_0)$. However, in an effort to understand the origin of the observed instability at small d_0, we will study the structural stability of the linearized eigenvalue problem by allowing $\eta(z)$ to be a random perturbation of the interface. Namely we shall slightly perturb the shape of the interface (which determines the kernel of the linearized eigenvalue problem) and look at the resulting change in the eigenspectrum. This will turn out to be exponentially sensitive on the amount of noise, i.e., the amplitude of $\eta(z)$.

The stability analysis is done by expanding Eq. (10) and keeping terms in ϵ, $d_0\epsilon$, and $\eta\epsilon$. Using Eq. (4) in Eq. (6) to compute $\tilde{\kappa}_t(z)$ to first order in ϵ and using the result in Eq. (10) one obtains after some lengthy algebra (the details of which will be presented elsewhere) the following set of linearized equations for the coefficients $\epsilon_n(t)$ [we have included the $O(d_0)$ correction to the finger shape, i.e., we let $\eta(z)\to\eta(z)+d_0\tilde{\kappa}_0(z)/2$]:

$$\frac{d\epsilon_l}{dt}=\sum_{n=1}^{\infty}\left[M_{ln}^0+\frac{d_0}{\pi}M_{ln}^1\right]\epsilon_n+\frac{d_0}{\pi}M_{ln}^2\epsilon_n^*\ , \tag{17}$$

where

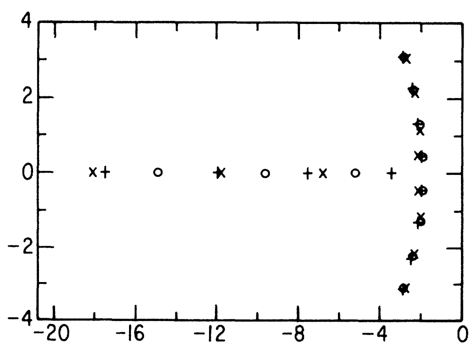

FIG. 2. Eigenspectrum at $d_0=0.05$ for various truncations: $N=130$ (+), $N=100$ (○), $N=80$ (×). Notice the discrete spectrum of asymmetric modes (complex eigenvalues) and the continuum of symmetric and antisymmetric modes (negative real eigenvalues).

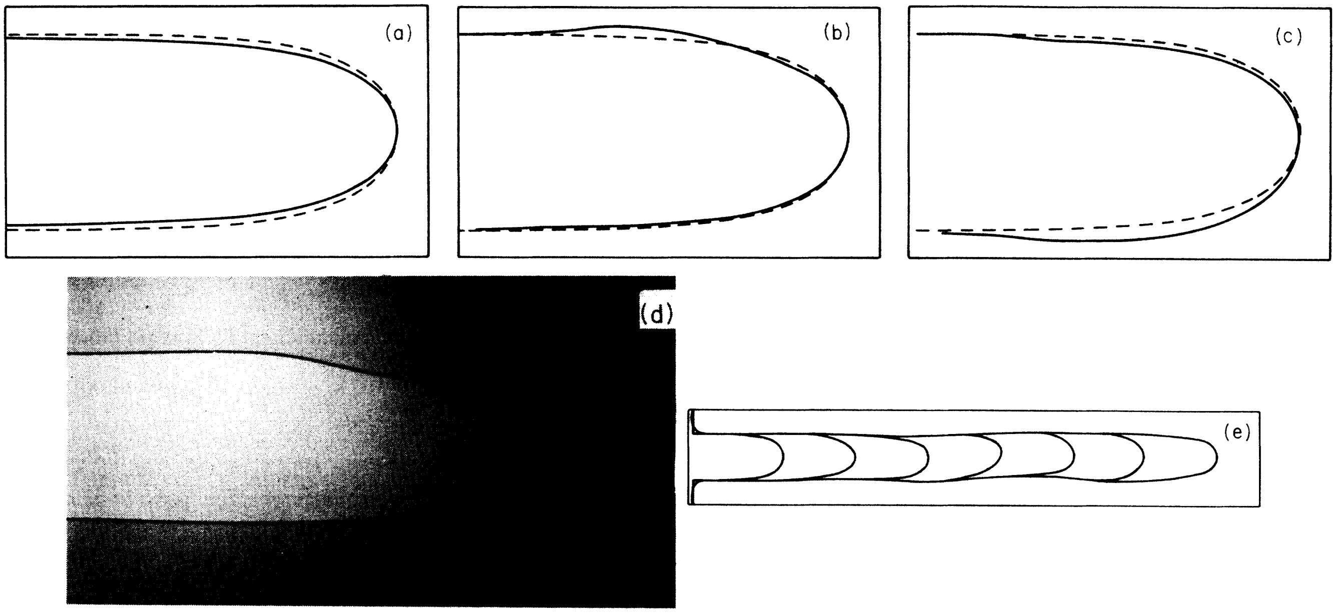

FIG. 3. Three most unstable modes (dashed line: unperturbed finger). (a) The symmetric nonoscillatory mode, which may be responsible for the experimentally and numerically observed fingers of width $\lambda < \frac{1}{2}$. (b) The asymmetric "hump" mode. (c) The asymmetric "tip wobbling" mode. (d) The asymmetric "hump" mode observed in an experiment [courtesy of P. Tabeling and A. Libchaber (Ref. 6). (e) Result of a Monte-Carlo simulation of the flow exhibiting the two asymmetric modes [courtesy of S. Liang (Ref. 13)].

$$M^0_{ln} = 2[l\delta_{ln} - (l+1)\delta_{l+1,n}] ,$$

$$M^1_{ln} = n[(A^+_{nl} - A^+_{n,l+1}) + (b_{n-l} - 2b_{n-l-1} + b_{n-l-2}) - 2(\bar\eta^*_{n-l+1} - 3\bar\eta^*_{n-l} + 3\bar\eta^*_{n+l-1} - \bar\eta^*_{n-l-2})] ,$$

$$M^2_{ln} = n[(A^-_{nl} - A^-_{n,l+1}) - (b_{n+l+1} - 2b_{n+l} + b_{n+l-1}) + 2(\bar\eta_{n+l+2} - 3\bar\eta_{n+l+1} + 3\bar\eta_{n+1} - \bar\eta_{n+l-1})] ,$$

with

$$A^\pm_{nl} \equiv l[(n+\tfrac{3}{2})\alpha^\pm_{n+1,l} - (n+\tfrac{1}{2})\alpha^\pm_{n,l}] ,$$

$$\alpha^\pm_{n,l} \equiv \frac{1}{\pm l - n + \frac{1}{2}} - \frac{1}{\pm l - n - \frac{1}{2}} ,$$

$$b_m \equiv -\frac{m}{m^2 - \frac{1}{4}} ,$$

and

$$\bar\eta_m \equiv \frac{\pi}{d_0} m \eta_m .$$

Notice that in the absence of surface tension ($d_0 = 0$) we recover the Saffman-Taylor results, the finger is linearly unstable (the matrix M^0_{ln} has eigenvalues equal to $2k$ where $k = 1, 2, 3, \ldots$). Also notice that the translational mode ϵ_0 decouples from these equations and is thus manifestly marginal. The eigenvalues of the above linear set of equations were obtained by truncating the expansion ϵ_n to order N (for N in the range 50–200). (A standard EISPACK package was used to compute the eigenvalues and eigenmodes of the resulting matrices.) The eigenspectrum for $d_0 = 0.05$ is shown in Fig. 2. Notice the continuum of symmetric modes (ϵ_n real) and antisymmetric modes (ϵ_n imaginary) characterized by negative real eigenvalues preceded by a discrete set of asymmetric modes (ϵ_n complex) with complex eigenvalues. These asymmetric modes appear when $d_0 < 1$, i.e., when the flat interface becomes linearly unstable, and their number subsequently increases as $d_0 \to 0$. The eigenvalues were all found to have negative real part (i.e., the interface is stable) for values of d_0 down to 10^{-3}. However, the lowest (asymmetric) eigenmodes were extremely sensitive to the amplitude of the noise (i.e., the amplitude of η). In fact the amount of noise needed to drive them unstable decreases exponentially with d_0. In the analysis as well as in the numerical simulations η_m was a random variable either uniformly distributed in m or with a Gaussian distribution near $m = 0$, i.e., $\eta_m = \nu\,\mathrm{random}(m)$. [When η_m is real, the eigenvalues of the truncated Eq. (17) can be found faster by computing the eigenvalues of the two $N \times N$ matrices $M^0 + d_0 M^1/\pi \pm d_0 M^2/\pi$.] Let ν_c be the amplitude of the noise necessary to obtain marginal eigenvalues, then we found

$$\nu_c \sim d_0^{1/2} \exp(-\alpha d_0^{-1/2}) , \tag{18}$$

where $\alpha \approx 1.3$. (For example, at $d_0 = 10^{-2}$, $\nu_c \approx 5 \times 10^{-6}$.) This particular fit is suggested by an argument due to Zel'dovitch *et al.*,[11] which can be adapted to the Saffman-Taylor problem.[12] Other fits are possible, e.g., $\nu_c \approx \exp(-\gamma d_0^{-\beta})$, with $\beta \approx 0.61$, and $\gamma \approx 0.72$.

The most unstable modes are shown in Fig. 3; there are two asymmetric oscillatory modes, and a symmetric nonoscillatory one which corresponds to a change in the width λ of the finger. These modes have apparently been observed in numerical simulations[13] and in real experiments.[6] The extreme sensitivity of the spectrum on the noise we interpret as a structural instability of the Saffman-Taylor equations at high velocities. We conjecture that this structural instability is related to a finite-amplitude nonlinear instability of the propagating finger at low surface tensions (see Appendix), such as the one observed in numerical simulations by DeGregoria and Schwartz.[14] In order to test that conjecture we have simulated the time evolution of the Saffman-Taylor problem in the presence of noise.

V. NUMERICAL SIMULATIONS

The numerical algorithm implementing the conformal-mapping technique to the study of the evolution of the interface is straightforward. Given $f_t(z)$, compute the curvature $\kappa(s)$ defined in Eq. (4) (all spatial derivatives were evaluated by Fourier methods), then evaluate $\tilde{\kappa}(z)$ given by Eqs. (5) and (6) and use Eq. (10) to determine $f_{t+\delta t}(z)$ by some convenient integration scheme (we used a fourth-order Runge-Kutta code). However, due to the contraction of points along the interface (s is uniformly distributed on the unit circle but its image on the interface Γ is not), we initially encountered numerical instability problems arising from very-high-frequency noise. In order to overcome these problems we introduced a routine which is averaging the curvature and its derivative over an arc-length smaller than λ_c (typically $\lambda_c/5$). λ_c is the critical wavelength associated to the instability of a flat interface. This routine thus reduces the resolution of the method and is similar to the introduction of an underlying grid used in other numerical schemes.[8,13,14] [The overall code is still very effective being an $N \ln N$ algorithm (N being the number of Fourier modes used). All calculations were performed on a FPS-164 array processor.] Being aware of the danger that such a scheme may alter in an uncontrollable way the time evolution of the interface, we have checked our algorithm with the known results in the asymptotic regime ($t \to \infty$).

A typical outcome of such a simulation is shown in Fig. 4 and fits well the finger shape obtained by the phenomenological scaling hypothesis of Pitts.[15] The dependence of the finger width on the McLean-Saffman surface-tension parameter κ is shown in Fig. 5 and agrees

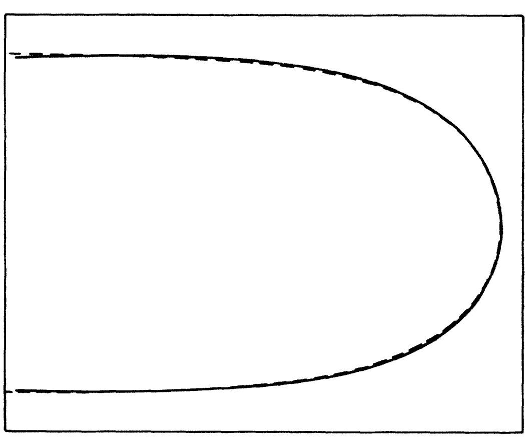

FIG. 4. Asymptotic ($t \to \infty$) finger for $d_0=0.04$ (solid line) compared with the asymptotic expected shape from Pitt's phenomenological scaling hypothesis (dashed line).

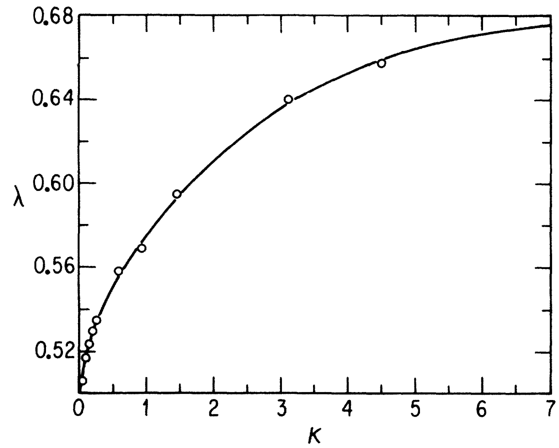

FIG. 5. Dependence of the finger width λ on the McLean-Saffman surface-tension parameter κ. The continuous curve is the McLean-Saffman relation.

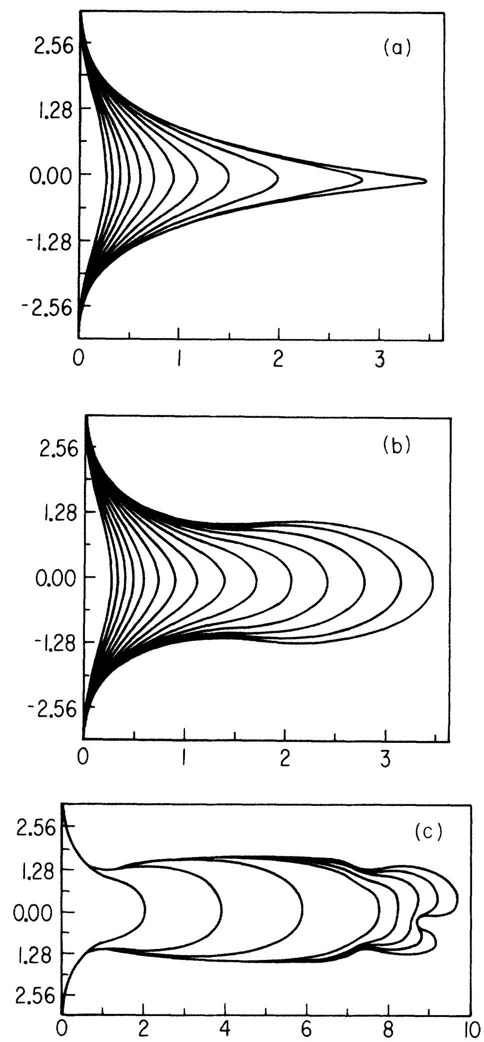

FIG. 6. Time evolution of arbitrary initial interfaces. (a) Evolution of an initial interface without surface tension. (b) Evolution of the same interface as in (a), but in the presence of surface tension ($d_0=0.01$). (c) Tip splitting in the evolution of an interface at low surface tensions ($d_0=0.01$).

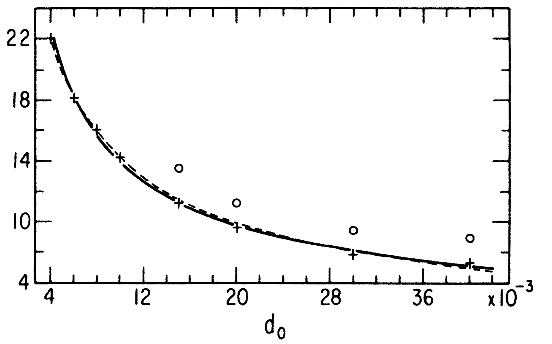

FIG. 7. Critical noise amplitude ν_c necessary to drive the system unstable as a function of the surface tension parameter d_0. Notice the vertical scale is logarithmic (we plot $-\log\nu_c$ vs d_0). The crosses (+) are results of the structural stability analysis, the continuous curve is a best fit of the form $\nu_c = \exp(-\gamma d_0^{-\beta})$ with $\beta = 0.61$ and $\gamma = 0.72$. The dashed line is a best fit of the form $\nu_c = \nu_c^0 d_0^{1/2} \exp(-\alpha d_0^{-1/2})$ with $\nu_c^0 = 26$ and $\alpha = 1.3$. The circles (O) are results of the numerical simulations which seemed to be more sensitive to noise by a constant factor.

with their numerical results for the steady-state interface. Finally in the absence of surface tension, the time evolution of the interface was in complete agreement with the exact time-dependent solutions.[7] It developed finite-time singularities, see Fig. 6(a). In its presence we could observe two regimes. One at low velocities ($d_0 > 10^{-2}$) for which an initial arbitrary interface evolves into the corresponding McLean-Saffman steady-state propagating finger, Fig. 6(b). The other at high velocities ($d_0 < 10^{-2}$) for which the finger is unstable, wobbling, and tip splitting, Fig. 6(c), this being in qualitative agreement with recent numerical and experimental work.[6,13,14,16]

We have then tested our conjecture that the instability of the finger in the second regime is due to numerical (or real) noise, and that the noise amplitude necessary to destabilize the finger decreases exponentially with increasing velocity [Eq. (18)]. This was done by looking for the onset of the instability—at a given value of d_0—as a function of the amplitude of a random analytic perturbation of the interface. In Fig. 7 are shown the results of the perturbation analysis and the numerical simulations. Both demonstrate the existence of a finite-amplitude nonlinear instability whose threshold is decreasing as an exponential of the velocity, i.e., as an exponential of $1/d_0$, though the numerical simulations seemed to be more sensitive to noise by a constant factor.

VI. CONCLUSION

We have argued for the existence in the Saffman-Taylor problem of a structural instability related to a nonlinear instability of the penetrating finger at low surface tensions. The most unstable modes predicted by our analysis are in good qualitative agreement with both experiment and numerical simulations. Finally, our numerical simulations confirm the existence of a nonlinear instability which threshold decreases exponentially with increasing velocity. A similar result was obtained by Zel'dovitch *et al.*[11] in the case of flame propagation in tubes. They found that the curved interface was stabilized due to the stretching of the perturbation wavelength by the tangential velocity component of the flow and the quenching by the walls. However, strong enough thermodynamic fluctuations could destabilize the flame front, their threshold amplitude decreasing exponentially with the Reynolds number. That argument can be adapted to the present case and yields a prediction similar to Eq. (18).[12]

ACKNOWLEDGMENTS

It is a pleasure to acknowledge a very fruitful collaboration and discussions with my advisor Leo Kadanoff, Boris Shraiman, Albert Libchaber, and Patrick Tabeling. I also benefited from discussions with H. Levine, D. Kessler, P. Pelce, and S. Liang. This work was supported by the Materials Research Laboratory of the University of Chicago under National Science Foundation Grant No. DMR-82-16892. This work was presented as a thesis to the Department of Physics, The University of Chicago, in partial fulfillment of the requirement for the Ph.D degree.

APPENDIX

We shall now argue for the existence of a relation between the structural stability of the linearized problem and the nonlinear instability of the full problem. Consider the following general equation:

$$\partial_t f = K(f) , \tag{A1}$$

where K is some nonlinear operator on f. That equation may have stable and unstable steady states f_s and f_u which means that the linear operator

$$L_{\bar f} = \left.\frac{\delta K}{\delta f}\right|_{\bar f}$$

has all its eigenvalues on the left of the complex plane at $\bar f = f_s$ and some eigenvalues on the right at $\bar f = f_u$. Notice that

$$0 = K(f_u) = \int_{f_s}^{f_u} L_\phi \, d\phi , \tag{A2}$$

where the integration is over a path in functional space from f_s to f_u. Since we expect the least-stable eigenmode to become unstable first (in particular, if it is well separated from the other modes), we may look for a path in functional space from f_s to f_u which at every point ϕ is tangential to the eigenmode μ of L_ϕ with maximal eigenvalue $\lambda_{\max}$ (i.e., the most unstable mode). Then parametrizing this path by t $[d\phi = \mu(t)dt]$ there exist some T such that

$$K(f_u) = \int_0^T \lambda_{\max}(t)\mu(t)dt = 0 . \tag{A3}$$

Thus we see that it may be possible from a structural stability analysis of the linearized problem L_ϕ, in the neighborhood ϕ of the linearly stable steady state f_s, to get information about the finite-amplitude nonlinear instability of f_s. If we are only interested in the scaling behavior of the critical destabilizing amplitude as a function of some parameter α, we may not have to calculate f_u as a function of α. Rather, we notice that the maximal eigenvalue of L_ϕ must change sign before f_u (i.e., for ϕ in a neighborhood of f_s not including f_u) so that we may sample the neighborhood of f_s and estimate the amplitude of the perturbation at which the linear operator L_ϕ has a marginal eigenvalue. The scaling of that amplitude (although dependent on the sampling scheme) yields qualitative information on the behavior of the critical destabilizing amplitude. And if only few modes are nonlinearly unstable such a sampling may project out a good approximation to the critical modes.

Example. In order to demonstrate the previous assertions let us consider the following simple nonlinear equation:

$$\partial_t x = -\delta x + y^3 ,$$

$$\partial_t y = x - y .$$

The stable steady state is at $f_s=(0,0)$. It has eigenvalues $\lambda_1=-\delta$, $\lambda_2=-1$, and associated eigenmodes $\mu_1=(1,1)$, $\mu_2=(0,1)$. Consider the path in functional space $\phi=f_s+t\mu_1$. The linearized operator is

$$L_\phi=\begin{bmatrix} -\delta & 3t^2 \\ 1 & -1 \end{bmatrix}$$

The maximal eigenvalue of L_ϕ is $\lambda_{\max}=-\delta+3t^2+O(\delta^2,t^4)$ and the associated mode is $\mu_1+O(\delta)$. To find the unstable steady state we look for T such that

$$O(\delta^2)=\int_0^T(-\delta+3t^2)dt .$$

The solution $T=\pm\delta^{1/2}$ implies that $f_u=(\pm\delta^{1/2},\pm\delta^{1/2})$ which, of course, is the known result. Notice that T is also the critical destabilizing amplitude. If we are only interested in the scaling of T as δ is decreased, then we may instead look at the scaling of T' where L_ϕ has a marginal eigenvalue, i.e., $T'=\pm(\delta/3)^{1/2}$. In that case the dependence of T and T' on δ is the same. This example demonstrates the relation between the structural stability analysis of the linearized problem, and the existence of a finite-amplitude nonlinear instability.

[1] H. J. S. Hele-Shaw, Nature **58**, 34 (1898).
[2] P. G. Saffman and G. I. Taylor, Proc. R. Soc. London Ser. A **245**, 312 (1958).
[3] J. W. McLean and P. G. Saffman, J. Fluid Mech. **102**, 455 (1981); J. W. McLean, Ph.D. thesis, California Institute of Technology, 1980.
[4] J.-M. Vanden-Broeck, Phys. Fluids **26**, 2033 (1983).
[5] D. A. Kessler and H. Levine, Phys. Rev. A **32**, 1930 (1985).
[6] P. Tabeling and A. Libchaber (unpublished).
[7] B. I. Shraiman and D. Bensimon, Phys. Rev. A **30**, 2840 (1984).
[8] G. Tryggvason and H. Aref, J. Fluid Mech. **136**, 1 (1983); J. Fluid Mech. (to be published).
[9] J.-M. Aribert, Ph.D. thesis, University of Toulouse, 1970.
[10] L. V. Ahlfors, *Complex Analysis* (McGraw-Hill, New York, 1953).
[11] Ya. B. Zel'dovitch, A. G. Istratov, N. I. Kidin, and V. B. Librovitch, Combust. Sci. Technol. **24**, 1 (1980).
[12] D. Bensimon, L. P. Kadanoff, S. Liang, B. I. Shraiman, and C. Tang (unpublished).
[13] S. Liang (unpublished).
[14] A. J. DeGregoria and L. W. Schwartz (unpublished).
[15] E. Pitts, J. Fluid Mech. **97**, 53 (1980).
[16] C.-W. Park and G. M. Homsy, Phys. Fluids **28**, 1583 (1985).

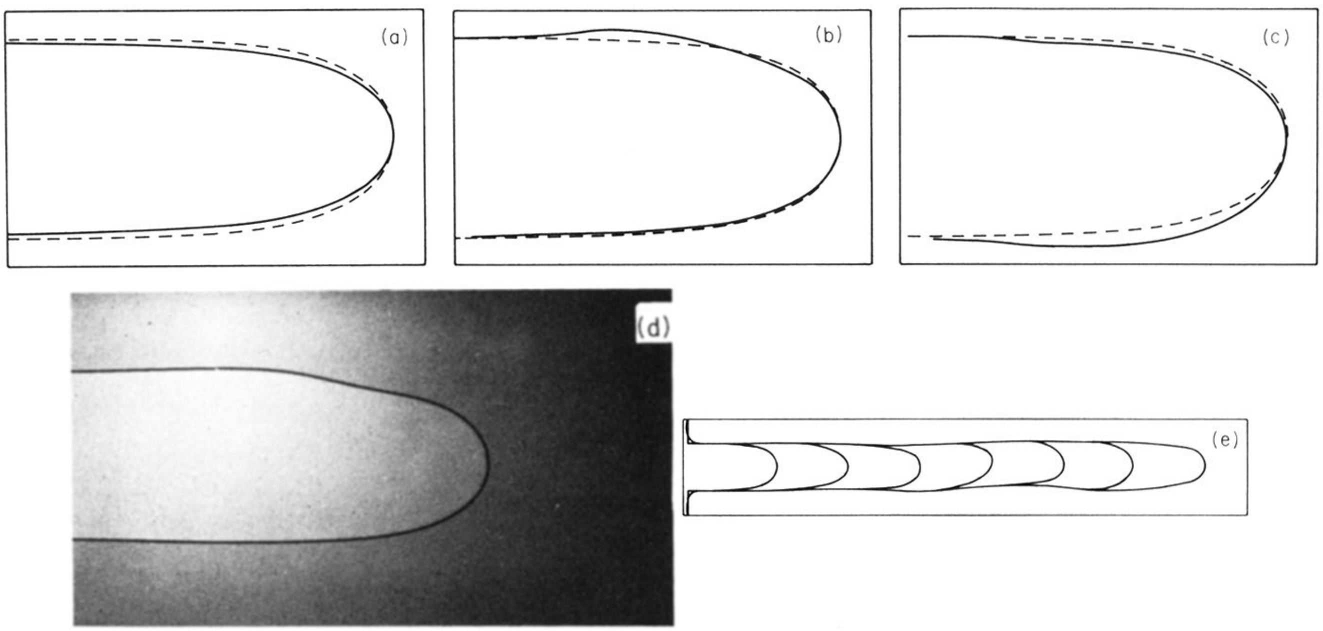

FIG. 3. Three most unstable modes (dashed line: unperturbed finger). (a) The symmetric nonoscillatory mode, which may be responsible for the experimentally and numerically observed fingers of width $\lambda < \frac{1}{2}$. (b) The asymmetric "hump" mode. (c) The asymmetric "tip wobbling" mode. (d) The asymmetric "hump" mode observed in an experiment [courtesy of P. Tabeling and A. Libchaber (Ref. 6). (e) Result of a Monte-Carlo simulation of the flow exhibiting the two asymmetric modes [courtesy of S. Liang (Ref. 13)].